Short-term variations in tracer tests responses in a highly karstified watershed

Vianney Sivelle, David Labat

Short-term variations in tracer tests responses in a highly karstified watershed

Vianney SIVELLE [(a)], David LABAT [(a)]

[(a)] Géosciences Environnement Toulouse, Université Toulouse 3 (Paul Sabatier)

REVISED VERSION FOR HYDROGEOLOGY JOURNAL

Manuscript number: HJ-2018-5698

Corresponding author:

Vianney SIVELLE

Géosciences Environnement Toulouse, Université Toulouse 3 (Paul Sabatier)

14, avenue Edouard Belin, 31400 Toulouse

(+33) 5.61.33.46.04

vianney.sivelle@get.omp.eu

Abstract

Modelling non-reactive solute transport based on artificial tracer tests have been widely used in the past decades. The dependence of solute transport from boundary conditions have been investigated across different hydrological conditions (low and high-water level) but still not investigated on short-term scale (i.e. hourly and daily scale). In this study, a campaign of several tracer tests is performed on a few days to investigate the short-term variations of tracer tests responses in a conduit dominated kart system during a recession without the influence of rainfall. Also, an improved artificial tracer test interpretation using a process engineering tool is introduced. It consists of a Laplace-transform transfer function approach of the residence time distribution curve. Considering the karstic system as a chemical reactor, the introduction of a transfer function approach appears to be an efficient way to describe the solute transport. Moreover, the transfer function is parametrized depending on the spring discharge. Finally, the model is extended to deal with source pollution scenario testing.

Keywords: artificial tracer test, karstic system, transfer function, pollution scenario

1 Introduction

Karstic systems consist of calcareous formations (carbonate rocks) in which the karstification process takes place. Three types of energy must be dispelled (Quinif, 1999): (1) mechanical actions create fissures and fractures that constitute a preferential underground pathway for water; (2) water-dissolved CO_2 reacts with carbonate rocks, and CO_2 partial pressure governs the rock dissolution potential (Dreybrodt, 1988); (3) water flows due to a hydraulic gradient between the inlet and outlet of the system (Mangin, 1975). This gradient controls water flow and dynamics in karstic systems (Delannoy, 1997; Jeannin, 1998; Mangin, 1984). Then, the process of karstification generates a subterranean network of cavities and drifts. This also leads to typical surface landscapes with geomorphological features such as dolines and karrens.

Artificial tracer tests is one of the most powerfull tools to study the conduit flow dynamics and have been widely used to study the solute transport in conduit dominated karst aquifers (Birk et al., 2005; Duran et al., 2016; Ender et al., 2018; Field and Pinsky, 2000; Goldscheider et al., 2008; Göppert and Goldscheider, 2007; Labat and Mangin, 2015; Massei et al., 2006; Morales et al., 2010). Solute transport is investigated under various hydrological conditions (i.e. low and high-water level, following “dry” or “rainy” periods). Then, modelling the solute transport includes knowledge about boundary conditions and their influence on the transport parameters (Cholet, 2017; Duran et al., 2016; Ender et al., 2018). This has been investigated over the hydrological cycle but remains not investigated on a short-term scale (i.e. hourly and daily scale).

To improve the understanding of the effect of short-term variations in boundary conditions, 11 tracer tests were performed over two weeks without significant influence of rainfall. These operations were performed with a certain temporal repartition to investigate the hourly and daily change in tracer tests response. We assume to summarize variations in boundary conditions through variations in the spring discharge. Also, as the tracer tests were performed in close hydrological conditions, we attempt to discriminate the effect of short-term

variation in tracer test response. Therefore, the following items are examined: (1) a transfer function approach is introduced to simulate non-reactive solute transport in a highly karstified watershed; (2) assessment of short-term (from hourly to daily scale) variations in tracer tests responses and (3) a new method is proposed to predict the solute transport between a preferential infiltration point in the watershed (typically a loss) and the outlet of the watershed.

2 Materials and methods

2.1 Artificial tracer tests in karstic systems

Artificial tracer tests enable analysis of the time of transit of a tracer in a karstic system. Basically, it consists of an injection of a known quantity of tracer, and the careful analysis of the curve for tracer restitution at the outlet, often called a tracer breakthrough curve (BTC). If a mass of tracer denoted *M* is added to the system at time t = 0, then the concentration at the outlet will be a function of time, denoted $C_{out}(t)$. After an infinite time, because of mass conservation, the recovered mass of tracer is given by Eqn (1).

$$\boldsymbol{M = \int_{t=0}^{t=\infty} C_{out}(t).Q(t).dt} \quad \textbf{(1)}$$

where $Q(t)$ is the spring flow as a function of time (m^3/s) and $C_{out}(t)$ is the concentration measured at the outlet of the system as a function of time (g/m^3). Because of natural heterogeneities and experimental approach, the mass conservation is rarely observed. Artificial tracer tests in karstic media often show a recovery of about 80% in high water level and around 20% in low water level. The reason of the discrepancy in recovery rate is still subject to investigation.

Fig. 1 shows a conceptual scheme for artificial tracer tests operated over a karstic system. The tracer response is formulated as an unsteady material balance, in terms of a linear differential equation with a constant coefficient that relates an input function $C_{in}(t)$ to a response function $C_{out}(t)$. The general form of the material balance is:

Inputs + Sources = Outputs + Sinks + Accumulations (2)

where inputs are the mass of tracer added by an operator, sources are the mass naturally present in the environment, outputs are the mass recovered at the measurement station, sinks are the mass reaching one or several non-monitored outlets of the drainage system and accumulations are the mass temporally stored in the drainage system. Sinks and accumulations can both be non-negligible in karstic systems. Considering multiple underground water pathways, part of the tracer could flow to sevral outputs (Luhmann et al., 2012) or could be temporally stored in immobile fluid regions (Dewaide et al., 2017; Goldscheider, 2008; Morales et al., 2010). Also, multiple peaked RTD curves could give evidence of multiple flow dynamics in the tracing system or multiple flow path (Field and Leij, 2012; Filippini et al., 2018; Vincenzi et al., 2011).

The residence time distribution (RTD), denoted $E(t)$ (s^{-1}), is derived from the concentration curve, denoted $C_{out}(t)$. It measures how long a tracer particle stays in the system and represents the probability density function for a water molecule to stay in the system during a period t (Jury and Roth, 1990). The $E(t)$ curve corresponds to normalization of the C curve to unity. Thus, in the case of a tracer system without dead space, the concentration can simply be divided:

$$\mathbf{E(t)} = \frac{\mathrm{C_{out}(t)}}{\mathbf{M/\nu}} = \frac{\mathrm{C_{out}(t).Q(t)}}{\int_{\mathbf{t=0}}^{\mathbf{t=\infty}} \mathrm{C_{out}(t).Q(t)dt}} \quad \text{where} \quad \int_{\mathbf{t=0}}^{\mathbf{t=\infty}} \mathbf{E(t)dt} = \mathbf{1} \qquad \textbf{(3)}$$

where $C_{out}(t)$ (t) is the concentration as a function of time (g/m^3), M is the mass of tracer injected (g) and ν is the mean flow rate (m^3/s). If the tracer is injected on period sufficiently short to be considered as instantaneous (i.e. the injection is close to a Dirac function) the observed RTD corresponds to the impulse response of the system.

One of the most frequently used methods for artificial tracer test interpretation is based on the advection-dispersion equation (ADE) introduced by Wang et al. (1987), and then

implemented in CXTFIT (Toride et al., 1995), QTRACER (Field, 2002; Field and Pinsky, 2000) and STANDMOD (Van Genuchten et al., 2012). The model is based on a dimensionless Peclet's numbers. It corresponds to the product of the length of flow and the mean velocity divided by the diffusivity and so roughly correspond to the Reynolds number but in term of porous media. ADE models allow determining the dispersivity coefficient which is dependent from boundary conditions (Duran et al., 2016; Massei et al., 2006) and from flow pathway (Ender et al., 2018; Lauber et al., 2014). The physical signification of parameters such as flow velocity and dispersivity can be questionable when it represents flow processes in karstic areas over several kilometres. Applications of ADE models assume that both the flow velocity and the dispersivity are constant in the system, but this is a condition rarely observed in karstic media. Because of high structural heterogeneities, the water flow velocity may present a spatial variation. This may influence the solute transport in the different compartment of the system (Ender et al., 2018). Nonetheless the physical signification of transport parameters in ADE models can be improved when the flow is segmented into sections, widely called "reach", where the flow conditions can be homogenous (Dewaide et al., 2017, 2016; Ender et al., 2018; Lauber et al., 2014). Here, as the underground drainage structure is not well constrained, a transfer function approach is chosen. It provides a framework including all processes (advection, diffusion, dispersion and mixing) in an assembly of conceptual reservoirs.

2.2 Tracer tests interpretation: a comparison with chemical engineering

Chemical engineering consists of all activities concerned with the exploitation of chemical reactions on an industrial scale (Levenspiel, 1999). These industrial processes are based on the concept of elementary reactors assembly to run material transformations. The flow behaviour of such reactors can be described based on a lumped model (Amin and Campana, 1996). This has been applied to the natural system, where the transit time can be estimated through the probability density function (PDF) of time residency (Bolin and Rodhe, 1973; Cornaton and Perrochet, 2006; Małoszewski and Zuber, 1982).

144 There may be several analogies between the structure present in karst aquifers and
145 chemical reactor. An empty tubular reactor can be simulated as a plug flow reactor, often
146 denoted as PFR (Walas, 2005). In karstic media, it corresponds to a piston effect (Bovolin et
147 al., 2017; Milanović, 2014). A stirred tank can be modelled by considering bypass zones,
148 stagnant zones and other parameters associated with the geometry of the vessels. In karstic
149 media, structures such as drains play the role of bypass zones, and annexe systems
150 constitute stagnant zones that could be connected to the main drainage system (Mangin,
151 1984; Marsaud, 1997). In the case of non-ideal reactors the flow conditions could be derived
152 from tracer test operations. The experimental RTD shape gives information about the main
153 flow and transport processes (Levenspiel, 2012; Walas, 2005).

154 As suggested by Becker and Bellin (2013), "*water moves through a series of different*
155 *elements that can be conceptualized as reservoirs or conduits, such as the epikarst,*
156 *fractures, open joints, pipes, solution conduits, pools, etc*". By analogy with process
157 engineering, a karstic system can be assimilated to a reservoir or an assembly of elementary
158 reservoirs. In this way, a karstic system could be studied as if it was a chemical reactor.
159 Nonetheless, in the case of a fluorescent dye tracer test, there is no material transformation
160 along water flow. Here, we focus on an approach widely used in chemical engineering to
161 study flow dynamics in chemical reactors from tracer tests. We do not consider any material
162 transformation but only mixing and transport.

163 Otherwise, this approach suffers from certain limitations. In industrial process engineering,
164 the chemical reactors characteristics are known. So, the chemical reactors are designed to
165 meet clearly-defined expectations. Then, tracer tests allow checking that reactors respond to
166 these expectations. On the contrary, in the karstic system study, it is difficult to understand
167 the geometrical arrangement of subterranean water flow. So, here it is proposed to use a
168 process engineering approach for interpretation of artificial tracer tests in a conduit
169 dominated karstic aquifer.

2.3 Proposal for a reservoir model for solute transport in conduit dominated flow

As shown in the previous part, karstic systems can be considered as an assembly of elementary reservoirs: water mixing takes place in a different compartment of the karstic system, leading to transformations between input and output signals. In this study, only the mixing between water and fluorescent dyes is considered. The input signal is a Dirac function, i.e. the injection period is extremely short compared to the mean residence time of the tracer in the system. The output signal is the experimental RTD derived from the concentration curve (BTC). The ratio between the input signal and the output signal in the Laplacian concept is called the transfer function, denoted H(p) (Walas, 2005):

$$\mathbf{H(p) = C_{out}\,(p)/C_{in}(p)} \quad \textbf{(4)}$$

$$\mathbf{H(p) = \mathcal{L}\{H(t)\} = \int_0^{\infty} e^{-p.t}.H(t).dt} \quad \textbf{(5)}$$

where $C_{in}(p)$ is the Laplace transform of the entrance, $C_{out}(p)$ is the Laplace transform of the outlet, *p* is the Laplace complex variable and $\mathcal{L}\{H(t)\}$ is the Laplace transform of the $H(t)$ function. Also, *E*(*t*) and $C_{out}(t)$ differ only by a constant, and the Laplace transform of a Dirac function is equal to 1. The a synthetic RTD, denoted *E**(*t*), can be calculated from the inverse Laplace transform of the transfer function with the Mellin's inverse formula:

$$\mathbf{E^*(t) = \mathcal{L}^{-1}\{H(p)\} = \frac{1}{2\pi i}\lim_{T\to\infty}\int_{\gamma-iT}^{\gamma+iT} e^{p.t}\,.C_{out}(p).dp} \quad \textbf{(6)}$$

where $E^*(t)$ is the simulated RTD in response to a Dirac function input for a system whose transfer function is *H*(*p*), and $\mathcal{L}^{-1}\{H(p)\}$ is the inverse Laplace transform of the $H(p)$ transfer function. *H*(*p*) is also called the impulse response of the system.

The transfer function formalism has been little used for artificial tracer test interpretation in karstic area. Only a few studies proposed this approach. Leibundgut (1998) proposed a dimensionless transfer function linking the peak of concentrations, the time of tracer peak and the standard deviation of the mean residence times to the discharge. Then, a synthetic tracer BTC can be proposed. Becker and Bellin (2013) proposed a conceptual model based on an assembly of several reservoirs in series, partitioning mass transfer between mobile and immobile zones. It consists of the transfer function approach of the Mobile-Immobile Model (Toride et al., 1993). Labat and Mangin (2015) split mass-transfer between fast and slow component. Nonetheless, their transfer function does not include a piston effect allowing to model the delay between slow and fast component. If tracer particles are transported by different flow dynamics, why do both slow and fast component restitutions start at the same time?

In this study, two perfect reactor models are considered: the plug flow reactor (PFR) and the mixed flow reactor (MFR). The corresponding transfer function is given in Eqn (7) and Eqn (8) (Levenspiel, 2012; Walas, 2005).

- mixed flow reactor (MFR):

$$\mathbf{H(p)} = \frac{\mathbf{1}}{\mathbf{1+\bar{t}*p}}$$

(7)

- plug flow reactor (PFR):

$$\mathbf{H(p)} = \mathbf{exp}\ (-\bar{\mathbf{t}} * \mathbf{p}) \qquad \textbf{(8)}$$

where $\bar{t}$ is the mean residence time.

Here, we propose a composite transfer function corresponding to an assembly of MFR and PFR:

$$\mathbf{H(p)} = \sum_{\mathbf{i=1}}^{\mathbf{k}} \left[\boldsymbol{\alpha}_\mathbf{i} * \left(\frac{\mathbf{1}}{\mathbf{1+ A^i * p}} \right)^{\mathbf{N}} * \mathbf{exp}\ (-\boldsymbol{\tau}_\mathbf{i} * \mathbf{p}) \right] \qquad \textbf{(9)}$$

where:

- k is an integer value corresponding to the number of flow components used in the model. So, it allows an extension of the model in case of complex RTD curves, with multiple parallel flow components due to friction effects (Massei et al., 2006) or flow partition between fast and slow flow (Labat and Mangin, 2015).

- α_i consists in the contribution of the flow component in the total tracer recovery and by construction $\sum \boldsymbol{\alpha_i} = \int_{\mathbf{t=0}}^{\mathbf{t=\infty}} \mathbf{E(t)dt} = \mathbf{1}$

- A is the mixing coefficient. In case of a perfect mixed flow reactor, it is equal to the mean time of residence of the tracer in the system. The corresponding transfer function is given in Eqn (7) (Levenspiel, 2012).

- N corresponds, from a conceptual point of view, to several reservoirs in cascade. In case of N is an integer value, it corresponds to a Nash cascade (Nash, 1957). Here, the Laplace framework allows to easily handle cases with non-integer N values belonging to R^+.

- τ is the time of transit for each of the sub-function. That is the time between the injection of the tracer into the system and its detection at the outlet. This is a delay which is classically expressed by an exponential function with a negative coefficient in the Laplace plane. When τ is equal to the mean time of residence, it corresponds to a PFR whose transfer function given in Eqn (8).

As the inverse Laplace transform cannot be operated analytically, we use the algorithm described by De Hoog et al. (1982) and implemented in MATLAB by Hollenbeck (1998). Then, an optimization procedure allows the definition of the best parameters for the model. This consists of the application of a particle swarm optimization (PSO) procedure (Kennedy and Eberhart, 1995) implemented in MATLAB (Global Optimization Toolbox). The cost function to reduce between observed and simulated RTD curves is based on a normalized root mean square error (NRMSE).

$$\mathbf{RMSE} = \sqrt{\frac{\sum_{\mathbf{i=1}}^{\mathbf{n}}(\mathbf{y_{obs}(i)} - \mathbf{y_{sim}\ (i)})^2}{\mathbf{n}}} \quad \textbf{(10)}$$

$$\mathbf{NRMSE} = \frac{\mathbf{RMSE}}{\mathbf{max(y_{obs})} - \mathbf{min(y_{obs})}} \quad \textbf{(11)}$$

where $y_{sim}(i)$ is the simulated discretized time series, $y_{obs}(i)$ is the observed discretized time series and n is the number of data.

At this stage, it is important to insist that 'tracing systems' should not be confused with 'karstic systems' as already mentioned in Fig. 1. Then, in term of transfer function approach, this implies that one transfer function runs for one tracing system whereas one karstic system can contain several tracing systems, and so must be described by several transfer functions that can be in series or in derivation.

3 Studied area and tracer test campaign

We applied the transfer function approach to several artificial tracer tests over the Baget karstic watershed (Fig. 2), part of the SNO Karst consortium (INSU-CNRS). This basin, located in the Pyrenees Mountains (Ariège, France), is characterized by a median altitude of about 940 m and an area of around 13 km^2. It belongs to the carbonated belt bordering the north of the French Pyrenees. The area is affected by the Alas fault: Jurassic to Cretaceous metamorphic limestone dips 45° to 75° under slaty flysch on the southern border. Jurassic and Palaeozoic metamorphic dolomite and flysch constitute the northern border of the watershed (Debroas, 2009). The valley is oriented in a west-east direction, following the contact between karstified calcareous formations and impervious flysch. In the upper part of the watershed, the Lachein river flows during periods of the high-water level. As mentioned by Mangin (1975) and Marsaud (1997), the Baget karstic system is composed of so-called "main drainage" and "annexe drainage" systems. The main drainage system consists of the most transmissive part with short residence time, whereas the annexe drainage system (ADS) would physically correspond to voids and caves connected to the main drainage systems characterized by a much longer residence time.

The Baget watershed has already been studied based on artificial tracer tests interpretation (Labat and Mangin, 2015). The study was based on classical artificial tracer tests with separated instantaneous injections. Here, a new field campaign is carried out with 11 tracer tests performed in April 2018 using fluorescein. Tracer tests were performed during a period without an important influence of rainfall, so there was not a high degree of fluctuation on the outlet discharge during the tracer recovery. During the tracer tests campaign the discharge rate varies from 0.9 m^3/s at the beginning of the first injection (used as calibration tracer test) down to around 0.45 m^3/s at the beginning of the second injection campaign. Then the discharge rate has gradually decreased down to 0.3 m^3/s at the end of the campaign. Therefore, the discharge rate has decreased by 33% during the 7 days long tracer tests campaign. A field fluorimeter GGUN-FL30 (Schnegg, 2002) was installed in station B1 on the 12^{th} of April 2018 and programmed to measure on a 15 minutes sampling rate until the 21st of April 2018. During the same period, the time interval for water sampling was adjusted for 60 minutes. Fluorescence measurement and water sampling were done near the station B1, where the discharge is measured since the late 1970s (Mangin, 1975). Water samples were analysed by the CETRAHE laboratory (Orléans, France) using spectrofluorimeter Hitachi F2500 and F7000. The characteristics of tracer tests are summarized in Table 1, and the injection-recovery (RTD) time series are placed in the rainfall-runoff time series in Fig. 3.

The injection point, called P2 Loss, was chosen so the tracer reached the subterranean drainage system rapidly. This led us to approach instantaneous injection (Dirac function) which is the basic hypothesis for artificial tracer tests interpretation. Both injection site, called P2 Loss, and recovery site, called B1, are in the downstream part of the watershed (Fig. 2). It is characterized by the presence of losses and of temporary or permanent resurgences in a spatially limited area of about 2 km^2. We should note that, during periods with high water levels, P2 Loss could run as a temporary resurgence. During tracer tests it was running as a loss, allowing quick tracer infiltration in the drainage system.

The tracer tests were performed on a period overlapping two states of the watershed: (1) from the 8 April 2018 to the 17 April 2018 the temporary resurgence of Moulo de Jaur is activated (Figure 2 - b) and (2) as the water level dropped, the temporary resurgence is deactivated until the end of the tracer tests. As the tracer tests were performed during a period overlapping the transition between these two states of the watershed, we try to assess if this change in the global hydrodynamic behaviour has an impact on the solute transport through artificial tracer tests responses.

4 Results

4.1 Calibration of the transfer function parameters

The first tracer test was performed on the 12 April 2018 as a classical artificial tracer test operation. This tracer test has two goals: (1) it gives preliminary information about flow dynamics to prepare the tracer tests campaign and (2) it is used to calibrate the transfer function model. The injection of 500 g of fluorescein is made in P2 Loss on a short period to get close from a Dirac function. Then, any other injection was performed before tracer concentration back to zero. The BTC shows a maximum concentration value of 23.7 µg/L and a strong asymmetry with a rapid climb lasting about 3 hours and an important tailing effect lasting about 65 hours long. This can be interpreted as the coexistence of multiple flow processes: (1) a fast flow component with rapid transit time dominated by a plug flow effects leading to a high tracer concentration on a short period and (2) a slow flow component dominated by mixing and diffusivity leading to less important concentration on longer period (Labat and Mangin, 2015; Massei et al., 2006). Also, tailing effects can be associated with the existence of immobile water zone, corresponding to dead spaces were part of the tracer mass could be temporarily stored (Becker and Bellin, 2013; Field and Leij, 2012; Goldscheider, 2008; Zhao et al., 2017).

The first tracer test is used to calibrate the transfer function parameters using PSO procedure (Fig. 4). The simulated RTD is composed of three sub-functions. These sub-functions, noted from component 1 to component 3, represent respectively 40%, 32% and

28% of the total mass transport. These successive sub-functions show a different time of transit in the studied tracing system, namely the volume of the drainage system sought during mass transport between the injection site and recovery site. The transit time of the first component is 75 min whereas the transit time for the two following sub-functions are respectively about 92 min and 110 min. Then, considering an apparent distance of 850 m between injection and recovery sites, the apparent flow velocity is respectively of 11.3 m/min, 9.2 m/min and 7.8 m/min. Also, the mixing coefficient A is equal to 47.8 and N is equal to 3.88. These coefficients are in the same order of magnitude as for the Norville chalk aquifer when the spring discharge is high (Sivelle et al., 2018).

Following this first tracer test, ten other tracer injections were performed at various time interval constituting a complex input signal. Each of these injections is made on a short period to get close from a Dirac function, in the same way as for the calibration tracer test. As the time between each injection is low, there is overlapping of BTC at the outlet. Also, as there is no rainfall during tracer tests, the temporal variation in boundary conditions might be summarized through outlet discharge decrease because of the watershed emptying. This has been observed on the field through the deactivation of the temporary resurgence called Moulo de Jaur (Fig 2 - b). Then, the output signal is deconvoluted using transfer function approach to identify the RTD associated to each tracer injection and to highlight potential non-stationarity or non-linearity.

4.2 Running deconvolution of the RTD

To estimate the outlet recovery signal, one needs to run a convolution with the transfer function model. Here, we cannot run a classical convolution operator as the signal is composed of a succession of so-called Dirac function. As for each injection all frequency is sought this could not be described with a Fourier transform. Here, the simulated output signal is considered as a summation of the contribution of the RTD corresponding to each tracer injection shifted in time on the total signal measured at the outlet.

In case of a linear system, with steady-state conditions, the transfer function of a system must be efficient regardless of time and of boundary conditions. Dealing with a natural flow in karstic aquifers is a complex task because temporal and spatial variations in boundary conditions may have a strong effect on the solute transport. Several studies have shown the effect of boundary conditions variations on solute transport based on artificial tracer tests performed in contrasted hydrological conditions. The variability of solute transport between high and low water level is well documented in the literature (Doummar et al., 2018; Duran et al., 2016, 2015; Ender et al., 2018). Also, these studies deal with solute transport variability at the hydrological cycle. In this study, artificial tracer tests were carried out in a few days period, without the influence of rainfall. Otherwise, the Baget watershed is not subject to tidal influence that can influence flow transport on the half-daily scale (Duran et al., 2016). So, as the hydrological conditions appear to be quite similar for each tracer tests, it could be possible to analyse more precisely the effect of conduit flow dynamics on the solute transport in the karstic conduit at hourly scale.

To investigate if solute transport can be influenced at a flood scale, the hypothesis of the linearity and stationarity of the system has been tested (Fig. 5 - A). If solute transport is considered not to be influenced by short-term variations in boundary conditions, at a daily scale, initial calibration of the transfer function appears not to be enough to model the outlet signal. Also, the variation in travel time might be considered in the transfer function (Fig. 5 – B). So, one needs to find the relation between transit time and discharge rate. Here, as all tracer tests were performed in close hydrological conditions, the relation between outlet discharge rate and transit time might be quite simple. As there is no important variation of the spring discharge, we could consider that the discharge measured at the outlet can be enough to correctly describe tracer transit time between input and output of the studied tracing system. Transit time is determined from the BTC curve for tracer tests 1, 2, 3, 8 and 9. These tests were performed such the tracer concentration at the outlet is sufficiently low to allow discrimination of a new arrival of the tracer. Transit time for tracer tests 4, 5, 6, 7, 10

and 11 could not be classically determined because of important interference of tracer restitution of each tracer injections. So, they have been determined from the experimental relationship between time of transit for tracer tests 1, 2, 3, 8 and 9 and corresponding outlet discharge. The relation is given by the Eqn (12) (Fig. 6).

$$\boldsymbol{\tau}\,(\mathbf{hour}) = \begin{cases} -\mathbf{33.72} * \mathbf{Q} + \mathbf{15.94}\,, & Qinj < 0.36\,m3/s \\ -\mathbf{4.02} * \mathbf{Q} + \mathbf{4.98}\,, & Qinj \geq 0.36\,m3/s \end{cases} \quad \textbf{(12)}$$

Where τ is the transit time (hour) and Q (m^3/s) is the discharge measured at the outlet when the tracer is added to the system. We have shown previously that the tracer tests were performed during a period overlapping a change in the global hydrodynamic watershed behaviour with deactivation of a temporary resurgence when the outlet discharge drops under 0.440 m^3/s. This is also observed in the apparent transport velocity of the tracer. So, the model is naturally composed of a linear relation with a different coefficient, depending if the temporary resurgence Moulo de Jaur is activated or not.

Also, it appears that the mixing coefficient shows variability depending on the outlet discharge rate. The previous study has shown that the mixing coefficient could be linked to the outlet discharge in case of a conduit dominated flow (Sivelle et al., 2018). As the discharge rate has decreased by 33% during the tracer tests campaign, the variation is considered sufficient to impact the solute transport. Here, the relation between the mixing coefficient A and the outlet discharge is considered as an *a priori* for the transfer function parametrization. Several regression equations have been tested and linear regression appears to be the more suitable solution. The parameters of the regression are part of the optimization procedure. Also, it allows reducing the number of parameters to optimize. Basically, the model needs an A value for each tracer injection, in this case 11. Here, it is reduced to 2 parameters and allow to expand the model for source pollution scenario testing for different outlet discharge rate. Then, the relation between the mixing coefficient and outlet discharge is given by Eqn (13) (Fig. 6).

$$\mathbf{A} = \mathbf{48.06} * \mathbf{Q} + \mathbf{14.89} \quad \textbf{(13)}$$

Where A is the mixing coefficient in the transfer function and Q (m^3/s) is the discharge measured at the outlet when the tracer is added to the system.

So, the transfer function now includes parameters variations directly linked to the boundary conditions, described through the outlet discharge. The transfer function is now expressed by Eqn (14).

$$\mathbf{H(p)} = \sum_{\mathbf{i}=1}^{\mathbf{k}} \left[\boldsymbol{\alpha}_{\mathbf{i}} * \left(\frac{1}{1 + \mathbf{A(q)}^{\mathbf{i}} * \mathbf{p}} \right)^{\mathbf{N}} * \exp\left(-\boldsymbol{\tau}(\mathbf{q})_{\mathbf{i}} * \mathbf{p} \right) \right] \quad \textbf{(14)}$$

As a result, considering the effects of changes in discharge rate allows a better simulation of the outlet signal (Fig. 5 - C). It appears that the transfer function might include part of the temporal variations of the boundary conditions, even at a recession scale. In this case it occurs on a few days without the influence of rainfall. It has been possible to find a relation between transfer function parameters and outlet discharge to improve the description of the solute transport in karst conduit. The output signal has been deconvoluted using a transfer function approach to identify each impulse response from a complex input signal. The signal has been simulated with an acceptable confidence level (NRMSE = 0.03 and NSE = 0.97) between observed and simulated data. Results of the parametrization are summarized in table 2 and corresponding normalized simulated RTD are shown in Fig. 7. Also, deconvolution of the global outlet signal allows discriminating the mixing effect of three different flow dynamics depending on the apparent velocity (Fig. 8). This differentiation in solute transport can be explained by friction effects (Massei et al., 2006) or by the spatial arrangement of the water flow throughout the transport between inlet and outlet (Field and Leij, 2012; Hauns et al., 2001)

4.3 Testing a pollution scenario

Considering the non-linear and non-stationary hydrodynamic behaviour in karst conduit, an efficient scenario testing should include these special features, and their influence on solute transport. Also, several questions must be answered in vulnerability assessment: (1) when the contamination will arrive at the target, (2) at what concentration level and (3) how long

427 the contaminant will last (Goldscheider, 2004; Iván and Mádl-Szőnyi, 2017). The VULK
428 method (Jeannin et al., 2001) was the first process based on vulnerability mapping. The main
429 idea of the method consists in modelling the breakthrough curve of a conservative
430 contaminant along the water pathway, separated in the sub-system. Nonetheless, the
431 possibility to consider a concentrated infiltration is not implemented into the original model. In
432 this study, a transfer function approach is used to model the solute transport in a karstic
433 area, based on artificial tracer tests performed from a loss, allowing quick infiltration in the
434 main drainage system. The model allows to correctly describe the residence time distribution
435 of a non-reactive tracer, and by extension of a potential contaminant with the same
436 behaviour. The model proposed here remains valid for solute transport occurring between
437 injection and recovery sites in a specific range of hydrological conditions. So, in term of
438 vulnerability assessment, the model proposed here may be classified as source vulnerability
439 and could help to prevent accidental pollution (Kavouri et al., 2011). As the model include a
440 dependence from the outlet discharge it is possible to investigate pollution scenario across
441 various hydrological conditions. The source vulnerability evolves across time depending on
442 the boundary conditions. These have an influence on a multi-temporal scale range, from the
443 daily scale (recessional following a rainfall event) to annual scale (between high and low
444 water level).

445 A primary approach in modelling RTD curves for various flood event consists in applying
446 transfer function approach to an input signal different from classical Dirac function
447 considering the discharge variation while tracer (or contaminant) is supposed to be added in
448 the system. Here, the solute transport transfer function proposed have been calibrated in a
449 specific range of spring discharge, during a recession where spring discharge decreases
450 from 0.9 m^3/s down to 0.3 m^3/s. The pollution scenario is tested on recession events with
451 spring discharge in the same order of magnitude. To do so, 17 recessions close to the one
452 observed during tracer tests have been identified (Fig. 9). These recessions checked the
453 following conditions: (1) the recession last more than four days, (2) the initial discharge is

about 0.9 m^3/s and (3) the final discharge is above 0.3 m^3/s. Thus, the scenario of pollution is tested in conditions close to the one investigated though artificial tracer tests. The scenario consists of infiltration at a constant concentration lasting 6 hours. As the recession coefficient varies between all the recession event, the effects of discharge decrease during contaminant infiltration and transport may be different. To asses these effects we ran the model on the 17 flood recessions and show some results in Fig. 10. The first scenario (Fig. 10 - a), with a mean discharge rate of around 0.7 m^3/s, shows that neglecting the discharge variation can lead to underestimating the peak of concentration. Nonetheless, in this scenario the time of transit and the duration of restitution appears to be quite good. Two other scenarios (Fig. 10 – b and c), with mean discharge rate of around 0.4 m^3/s, show that neglecting discharge variations can lead to significative errors in transit time estimation. This is a consequence of the ceiling effect present in Eqn 12 (Fig. 6) and highlights the effect of non-linearity in karstic media on solute transport.

5 Discussion

5.1 Model application

The model proposed here is based on a transfer function approach. The parametrization is derived from artificial tracer tests performed in close hydrological conditions. The main objective was to assess the effect of short-term variations in boundary condition on artificial tracer test response. One should keep in mind several limitations of the model.

The model remains valid as the hydrological conditions are closed to the one investigated during the field campaign. An extrapolation of the linear regression between transfer function parameters and spring discharge appears not to be relevant. Indeed, the Eqn (14) gives a negative transit time in case of the spring discharge is above 1.240 m^3/s, which is physically non-acceptable. So, an extension of the model to a lager range of hydrological conditions needs more field data to find a suitable model. The model consists of both the transfer function and the regression equation between transfer function parameters and the environmental variables. Here, only the influence of spring discharge has been investigated

but the model may be extended by integration of other variables such as piezometric level or tidal coefficient in case of coastal aquifers submitted to tidal influence.

The model offers a new way to deal with pollution scenario testing including a short-term variation of boundary condition on the solute transport. Users should keep in mind the range of hydrological conditions where the model has been calibrated. The validity domain of the model is strongly dependent on the range of hydrological condition investigated through artificial tracer tests. Also, the model is calibrated depending on the objective in term of source vulnerability characterization and depending on available data on the area.

6 Conclusion

In this paper, several problems with solute transport in karstic areas have been addressed: (1) solute transport modelling in karst conduit using a transfer function approach, (2) assessment of the short-term variations in tracer test responses and (3) testing accidental pollution scenario including discharge variations along the infiltration and restitution of the contaminant.

A transfer function approach is used for the RTD curves modelling from fluorescent dye tracer tests. It consists of a systemic approach, allowing inclusion of all processes in a conceptual reservoir model. The model introduced here is composed of 3 delayed sub-functions. The delay in solute transport can be explained by the existence of complex structure acting like dead zones (Becker and Bellin, 2013; Field and Pinsky, 2000; Goldscheider, 2008), by friction effects (Massei et al., 2006) or by partition in flow dynamics (Labat and Mangin, 2015). Flow dynamics in karst aquifers shows strong non-linearity: it may exist ceil effects depending on the activation or deactivation of flow path depending on the water table level. In this study, artificial tracer tests were performed during a period when one temporary resurgence (called Moulo de Jaur) has been deactivated. As a result, the regression equation between spring discharge and time of transit show different coefficient from either side of the spring discharge ceil, corresponding to the activation/deactivation of this temporary loss.

The main result of the study highlights the influence of short term variation in boundary condition on artificial tracer test response.. It constitutes a new way to deal with source pollution scenario. Considering one accidental pollution scenario lasting 6 hours over several quite similar recession event, it appears that the shape of the recession has an influence on solute transport. So, the model allows to include discharge fluctuation during solute transport (and by extension contaminant) and gives a better description of the recovery at the outlet. Omit the effects of short-term variations in boundary condition can lead to under-estimate the peak of concentration. Also, the time of transit and the time for maximal concentration reaching outlet can be badly estimated considering a constant discharge rate. Users should keep in mind the range of hydrological conditions where the model have been calibrated to ensure the model prevision is sufficiently reliable.

Acknowledgement

The authors would like to thank the KARST observatory network (SNO KARST) imitative at the INSU/CNRS, which aims to strengthen knowledge sharing and promote cross-disciplinary research on karst systems at the national scale. We also thank “Météo-France” for providing rainfall data and BRGM (French geological survey) for providing discharge data. This work has been funded by “l’Agence de l’eau Adour Garonne”.

References

Becker, M., Bellin, A., 2013. A reservoir model of tracer transport for karstic flow systems. Hydrogeol J 21, 1011–1019. https://doi.org/10.1007/s10040-013-0991-2

Birk, S., Geyer, T., Liedl, R., Sauter, M., 2005. Process-based interpretation of tracer tests in carbonate aquifers. Ground Water 43, 381–388. https://doi.org/10.1111/j.1745-6584.2005.0033.x

Bovolin, V., Cuomo, A., Guida, D., 2017. Hydraulic modeling of flood pulses in the Middle Bussento Karst System (MBSKS), UNESCO Cilento Global Geopark, southern Italy. Hydrol. Process. 31, 639–653. https://doi.org/10.1002/hyp.11056

Cholet, C., 2017. Fonctionnement hydrogéologique et processus de transport dans les aquifères karstiques du Massif du Jura (Thèse de Doctorat). Université de Bourgogne Franche-Comté.

De Hoog, F.R., Knight, J.H., Stokes, A.N., 1982. An improved method for numerical inversion of Laplace transforms. SIAM Journal on Scientific and Statistical Computing 3, 357–366.

Debroas, E.-J., 2009. Géologie du bassin versant du Baget (Zone nord-pyrénéenne, Ariège, France) : nouvelles observations et conséquences. Strata 2, 1–93.

Delannoy, J.-J., 1997. Recherches géomorphologiques sur les massifs karstiques du Vercors et de la transversale de Ronda (Andalousie) : les apports morphogéniques du karst (phdthesis). Université Joseph-Fourier - Grenoble I.

Dewaide, L., Bonniver, I., Rochez, G., Hallet, V., 2016. Solute transport in heterogeneous karst systems: Dimensioning and estimation of the transport parameters via multi-sampling tracer-tests modelling using the OTIS (One-dimensional Transport with Inflow and Storage) program. Journal of Hydrology 534, 567–578. https://doi.org/10.1016/j.jhydrol.2016.01.049

Dewaide, L., Collon, P., Poulain, A., Rochez, G., Hallet, V., 2017. Double-peaked breakthrough curves as a consequence of solute transport through underground lakes: a case study of the Furfooz karst system, Belgium. Hydrogeology Journal. https://doi.org/10.1007/s10040-017-1671-4

Doerfliger, N., Jeannin, P.-Y., Zwahlen, F., 1999. Water vulnerability assessment in karst environments: a new method of defining protection areas using a multi-attribute approach and GIS tools (EPIK method). Environmental Geology 39, 165–176.

Doummar, J., Margane, A., Geyer, T., Sauter, M., 2018. Assessment of key transport parameters in a karst system under different dynamic conditions based on tracer experiments: the Jeita karst system, Lebanon. Hydrogeol J 1–13. https://doi.org/10.1007/s10040-018-1754-x

Dreybrodt, W., 1988. Processes in Karst Systems - Physics, Chemistry, and Geology, Springer Series in Physical Environment. Springer-Verlag Berlin Heidelberg.

Duran, L., Fournier, M., Massei, N., Dupont, J.-P., 2016. Assessing the Nonlinearity of Karst Response Function under Variable Boundary Conditions. Ground Water 54, 46–54. https://doi.org/10.1111/gwat.12337

Duran, L., Fournier, M., Massei, N., Dupont, J.-P., 2015. Use of Tracing Tests to Study the Impact of Boundary Conditions on the Transfer Function of Karstic Aquifers, in: Hydrogeological and Environmental Investigations in Karst Systems, Environmental Earth

Sciences. Springer, Berlin, Heidelberg, pp. 113–122. https://doi.org/10.1007/978-3-642-17435-3_13

Ender, A., Goeppert, N., Goldscheider, N., 2018. Spatial resolution of transport parameters in a subtropical karst conduit system during dry and wet seasons. Hydrogeol J 1–15. https://doi.org/10.1007/s10040-018-1746-x

Field, M.S., 2002. The QTRACER2 program for tracer-breakthrough curve analysis for tracer tests in karstic aquifers and other hydrologic systems. National Center for Environmental Assessment–Washington Office, Office of Research and Development, US Environmental Protection Agency.

Field, M.S., Leij, F.J., 2012. Solute transport in solution conduits exhibiting multi-peaked breakthrough curves. Journal of Hydrology 440–441, 26–35. https://doi.org/10.1016/j.jhydrol.2012.03.018

Field, M.S., Pinsky, P.F., 2000. A two-region nonequilibrium model for solute transport in solution conduits in karstic aquifers.pdf. Journal of Contaminent Hydrology 44, 329–351.

Filippini, M., Squarzoni, G., De Waele, J., Fiorucci, A., Vigna, B., Grillo, B., Riva, A., Rossetti, S., Zini, L., Casagrande, G., Stumpp, C., Gargini, A., 2018. Differentiated spring behavior under changing hydrological conditions in an alpine karst aquifer. Journal of Hydrology 556, 572–584. https://doi.org/10.1016/j.jhydrol.2017.11.040

Ford, D., Williams, P.D., 2007. Karst Hydrogeology and Geomorphology. John Wiley & Sons, Inc.

Goldscheider, N., 2008. A new quantitative interpretation of the long-tail and plateau-like breakthrough curves from tracer tests in the artesian karst aquifer of Stuttgart, Germany. Hydrogeology Journal 16, 1311–1317. https://doi.org/10.1007/s10040-008-0307-0

Goldscheider, N., 2004. The concept of groundwater vulnerability., in: Vulnerability and Risk Mapping for the Protection of Carbonate (Karst) Aquifers, Final Report (COST Action 620) Report EUR 20912.

Goldscheider, N., Hötzl, H., Fries, W., Jordan, P., 2001. Validation of a vulnerabilty map (EPIK) with tracer tests. Presented at the Proc. 7th Conference on Limestone Hydrology and Fissured Media, Besançon, pp. 167–170.

Goldscheider, N., Meiman, J., Pronk, M., Smart, C., 2008. Tracer tests in karst hydrogeology and speleology. International Journal of Speleology 37, 3.

Göppert, N., Goldscheider, N., 2007. Solute and Colloid Transport in Karst Conduits under Low- and High-Flow Conditions. Ground Water 0, 071003004158004-??? https://doi.org/10.1111/j.1745-6584.2007.00373.x

Hauns, M., Jeannin, P.-Y., Atteia, O., 2001. Dispersion, retardation and scale effect in tracer breaktrough curves in karst conduits. Journal of Hydrology 241, 177–193.

Hollenbeck, K.J., 1998. INVLAP.M: A Matlab Function for Numerical Inversion of Laplace Transforms by de Hoog Algorithm. [WWW Document]. URL https://www.mathworks.com/matlabcentral/answers/uploaded_files/1034/invlap.m (accessed 12.7.16).

Iván, V., Mádl-Szőnyi, J., 2017. State of the art of karst vulnerability assessment: overview, evaluation and outlook. Environmental Earth Sciences 76. https://doi.org/10.1007/s12665-017-6422-2

Jeannin, P.-Y., 1998. Structure et comportement hydraulique des aquifères karstiques.

612 Université de Neuchâtel, Neuchâtel.

613 Jeannin, P.-Y., Cornaton, F., Zwahlen, F., Perrochet, P., 2001. VULK: a tool for intrinsic
614 vulnerability assessment and validation. Presented at the Proc. 7th Conference on Limestone
615 Hydrology and Fissured Media, Besançon, pp. 185–190.

616 Jury, W.A., Roth, K., 1990. Transfer functions and solute movement through soil: theory and
617 applications. Transfer functions and solute movement through soil: theory and applications.

618 Käss, W.A., 1994. Hydrological tracing practice on underground contaminations.
619 Environmental geology 23, 23–29.

620 Kavouri, K., Plagnes, V., Dörfliger, N., Faycal, R., Pierre, M., 2011. PaPRIKa: a method for
621 estimating karst resource and source vulnerability--application to the Ouysse karst system
622 (southwest France). Hydrogeology Journal 19, 339–353. https://doi.org/10.1007/s10040-010-
623 0688-8

624 Kennedy, J., Eberhart, R., 1995. Particle swarm optimization, in: , IEEE International
625 Conference on Neural Networks, 1995. Proceedings. Presented at the , IEEE International
626 Conference on Neural Networks, 1995. Proceedings, pp. 1942–1948 vol.4.
627 https://doi.org/10.1109/ICNN.1995.488968

628 Kovács, A., Perrochet, P., 2008. A quantitative approach to spring hydrograph decomposition.
629 Journal of Hydrology 352, 16–29. https://doi.org/10.1016/j.jhydrol.2007.12.009

630 Labat, D., Mangin, A., 2015. Transfer function approach for artificial tracer test interpretation
631 in karstic systems. Journal of Hydrology 529, 866–871.
632 https://doi.org/10.1016/j.jhydrol.2015.09.011

633 Lauber, U., Ufrecht, W., Goldscheider, N., 2014. Spatially resolved information on karst
634 conduit flow from in-cave dye tracing. Hydrology and Earth System Sciences 18, 435–445.
635 https://doi.org/10.5194/hess-18-435-2014

636 Leibundgut, C., 1998. Vulnerability of karst aquifers. IAHS PUBLICATION 247, 45–60.

637 Levenspiel, O., 2012. Tracer Technology, Fluid Mechanics and Its Applications. Springer
638 New York, New York, NY. https://doi.org/10.1007/978-1-4419-8074-8

639 Levenspiel, O., 1999. Chemical reaction engineering, 3. ed. ed. Wiley, Hoboken, NJ.

640 Luhmann, A.J., Covington, M.D., Alexander, S.C., Chai, S.Y., Schwartz, B.F., Groten, J.T.,
641 Alexander Jr., E.C., 2012. Comparing conservative and nonconservative tracers in karst and
642 using them to estimate flow path geometry. Journal of Hydrology 448–449, 201–211.
643 https://doi.org/10.1016/j.jhydrol.2012.04.044

644 Mangin, A., 1994. Karst Hydrogeology, in: Danielopol, D.L., Stanford, J.A. (Eds.),
645 Groundwater Ecology. Academic Press, San Diego, pp. 43–67.

646 Mangin, A., 1984. Pour une meilleure connaissance des systèmes hydrologiques à partir des
647 analyses corrélatoire et spectrale. Journal of Hydrology 67, 25–43.
648 https://doi.org/10.1016/0022-1694(84)90230-0

649 Mangin, A., 1975. Contribution à l'étude hydrodynamique des aquifères karstiques (Thèse de
650 Doctorat). Université de Bourgogne.

651 Marín, A.I., Andreo, B., Mudarra, M., 2015. Vulnerability mapping and protection zoning of
652 karst springs. Validation by multitracer tests. Science of The Total Environment 532, 435–
653 446. https://doi.org/10.1016/j.scitotenv.2015.05.029

654 Marsaud, B., 1997. Structure et fonctionnement de la zone noyée des karsts à partir des

résultats expérimentaux (Thèse de Doctorat ès Sciences). Université de Paris XI Orsay, Paris.

Massei, N., Wang, H.Q., Field, M.S., Dupont, J.P., Bakalowicz, M., Rodet, J., 2006. Interpreting tracer breakthrough tailing in a conduit-dominated karstic aquifer. Hydrogeology Journal 14, 849–858. https://doi.org/10.1007/s10040-005-0010-3

Matsubayashi, U., Velasquez, G.T., Takagi, F., 1993. Hydrograph separation and flow analysis by specific electrical conductance of water. Journal of Hydrology 152, 179–199.

Milanović, P., 2014. Hydraulic Properties of Karst Groundwater and Its Impacts on Large Structures, in: Mudry, J., Zwahlen, F., Bertrand, C., LaMoreaux, J.W. (Eds.), H2Karst Research in Limestone Hydrogeology. Springer International Publishing, Cham, pp. 19–48. https://doi.org/10.1007/978-3-319-06139-9_2

Morales, T., Uriarte, J.A., Olazar, M., Antigüedad, I., Angulo, B., 2010. Solute transport modelling in karst conduits with slow zones during different hydrologic conditions. Journal of Hydrology 390, 182–189. https://doi.org/10.1016/j.jhydrol.2010.06.041

Moser, H., 1995. Groundwater tracing, in: Tracer Technologies for Hydrological Systems. Presented at the Proceedings of a Boulder Symposium, IAHS.

Nash, J.E., 1957. The form of the instantaneous unit hydrograph. International Association of Scientific Hydrology, Publ 3, 114–121.

Padilla, A., Pulido-Bosch, A., 1995. Study of hydrographs of karstic aquifers by means of correlation and cross-spectral analysis. Journal of Hydrology 168, 73–89.

Perrin, J., Pochon, A., Jeannin, P.-Y., Zwahlen, F., 2004. Vulnerability assessment in karstic areas: validation by field experiments. Environmental Geology 46. https://doi.org/10.1007/s00254-004-0986-3

Quinif, Y., 1999. Karst et évolution des rivières : le cas de l'Ardenne. Geodinamica Acta 12, 267–277.

Ravbar, N., Goldscheider, N., 2009. Comparative application of four methods of groundwater vulnerability mapping in a Slovene karst catchment. Hydrogeology Journal 17, 725–733. https://doi.org/10.1007/s10040-008-0368-0

Schnegg, P.-A., 2002. An inextensive field fluorometer for hydrogeological tracer tests with three tracers and turbidity measurement, in: Groundwater and Human Development. Presented at the XXXII IAH and ALHSUD congress, Bocanegra, E - Martinez, D - Massone, H (Eds.), Balkema, Rotterdam, Mar del Plata, Argentina, pp. 1484–1488.

Sivelle, V., Labat, D., Duran, L., Masséi, N., Fournier, M., 2018. Artificial tracer tests interpretation using transfer function approach to study the Norville karst system, in: Eurokarst 2018 (in Press).

Toride, N., Leij, F.J., Van Genuchten, M.T., others, 1995. The CXTFIT code for estimating transport parameters from laboratory or filed tracer experiments. US Salinity Laboratory Riverside.

Toride, N., Leu, F.J., Van Genuchten, M.T., 1993. A Comprehensive Set of Analytical Solutions for Nonequilibrium Solute Transport With First-Order Decay and Zero-Order Production. Water Resources Research 29, 2167–2182.

Van Genuchten, M.T., Simunek, J., Leij, F.J., Toride, N., Sejna, M., 2012. STANMOD: Model use, calibration, and validation. Transactions of the ASABE 55, 1353–1366.

Vincenzi, V., Riva, A., Rossetti, S., 2011. Towards a better knowledge of Cansiglio karst

system (Italy): results of the first successful groundwater tracer test. Acta Carsologica 40.

Walas, S.M., 2005. Chemical reaction engineering handbook of solved problems. Gordon and Breach.

Wang, H.Q., Crampon, N., Huberson, S., Garnier, J.M., 1987. A linear graphical method for determining hydrodispersive characteristics in tracer experiments with instantaneous injection. Journal of Hydrology 95, 143–154. https://doi.org/10.1016/0022-1694(87)90121-1

Worthington, S.R., 2003. A comprehensive strategy for understanding flow in carbonate aquifer. Speleogenesis & Evolution of Karst Aquifers 1, 1–8.

Worthington, S.R.H., Ford, D.C., 2009. Self-Organized Permeability in Carbonate Aquifers. Ground Water 47, 326–336. https://doi.org/10.1111/j.1745-6584.2009.00551.x

Zhao, X., Chang, Y., Wu, J., Peng, F., 2017. Laboratory investigation and simulation of breakthrough curves in karst conduits with pools. Hydrogeology Journal 25, 2235–2250. https://doi.org/10.1007/s10040-017-1626-9

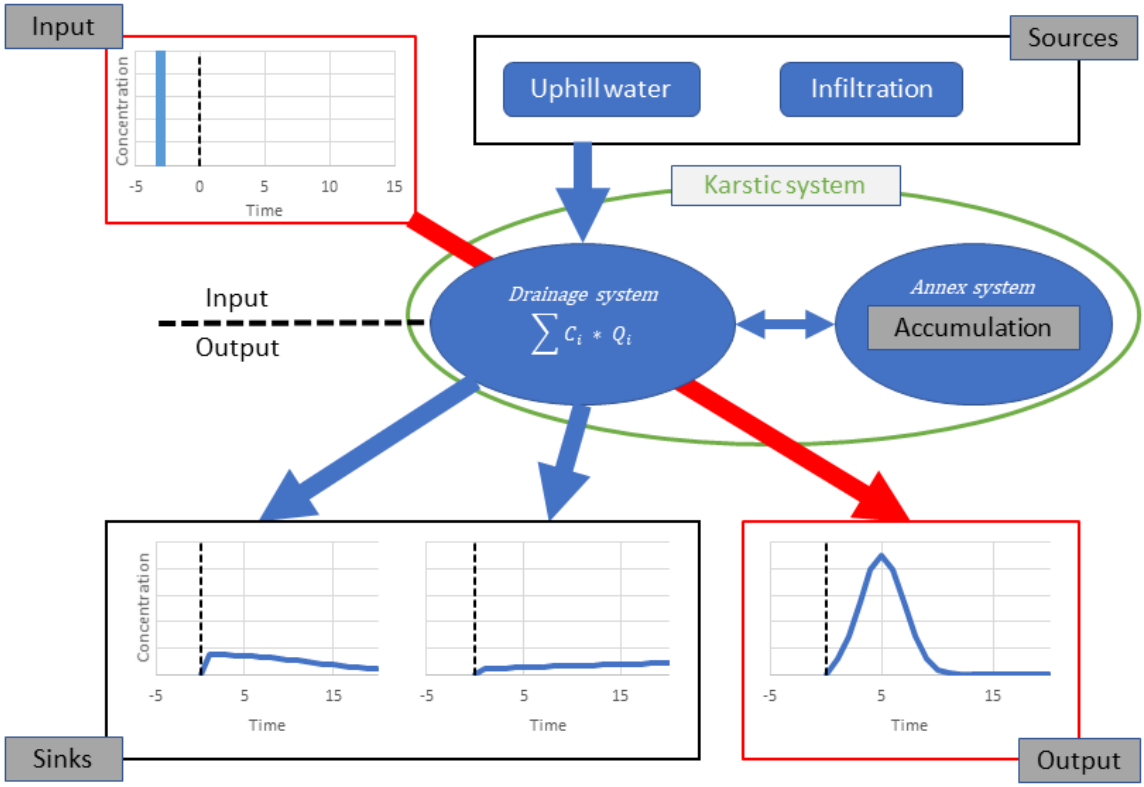

712

713 Fig. 1:

714 A conceptual model for artificial tracer tests interpretation using a transfer function approach.
715 The transfer function is used to model de solute transport in a tracing system, which
716 represents only a limited part of the karstic system, by considering the input/output relation
717 (systemic approach). The tracing system corresponds to the red arrow linking the input to the
718 output. Input consists of an instantaneous injection of a tracer mass injected by an operator.
719 Sources are equal to 0 for artificial tracer tests. It consists of the injection of fluorescent dyes,
720 normally nonexistent in natural conditions. By this way, the only mass of tracer present in the
721 system corresponds to the one introduced by the operator. The output is the tracer
722 breakthrough tracer curve measured at the monitored outlet of the karstic system.

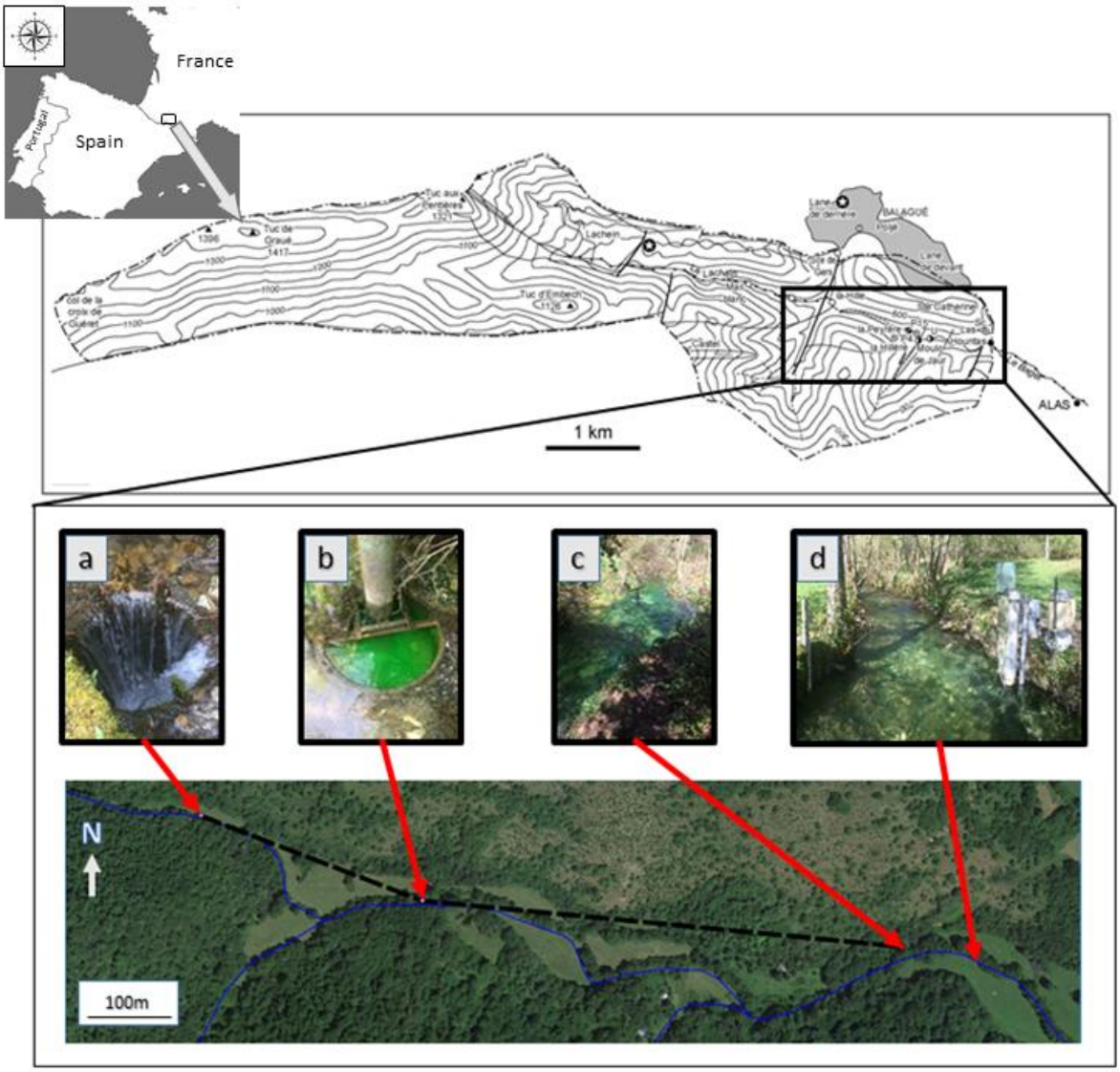

Fig. 2:

Top: localization of the Baget karstic system and description of the watershed which limits are represented by the *black dashed line*. The inlet and outlet tracer injection/recovery are in the upstream part of the basin (*black rectangle*).

Bottom: pictures of injection/recovery point over the area: a) P2 Loss is the point of injection, b) Moulo de Jaur is an intermediate observation point of the tracer transfer, c) Las Hountas is the recovery point and d) is the monitored station, denoted B1 (discharge, water sampling and fluorimeter).

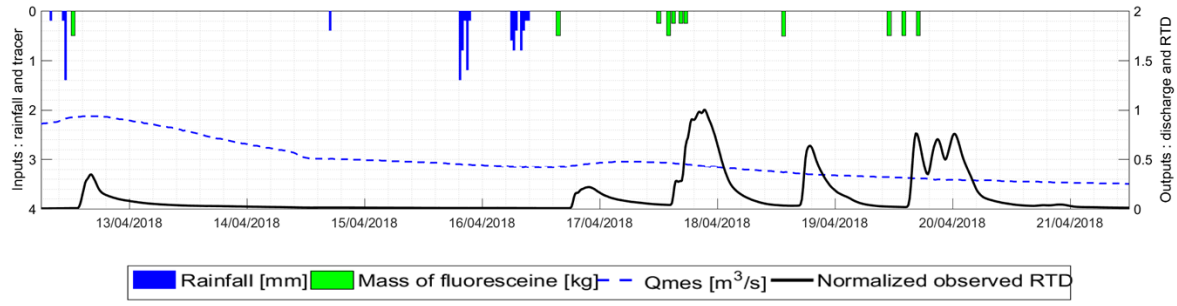

732

733 Fig. 3:

734 Rainfall-runoff time series on the Baget karstic watershed from 12 April to 22 April 2018.
735 Rainfall is measured by Meteo France at the Antichan station. Gauging station and
736 fluorimeter are located downstream Las Hountas. The successive injection of fluorescein and
737 residence time distribution are also reported in the same input-output format. Tracer tests
738 were performed in periods without the influence of rainfall. During the tracer tests campaign
739 the discharge rate varies from 0.9 m^3/s at the beginning of the first injection down to around
740 0.45 m^3/s at the beginning of the second injection campaign. Then the discharge rate has
741 gradually decreased down to 0.3 m^3/s at the end of the campaign. Therefore, the discharge
742 rate has decreased by 33% during the 7 days long tracer tests campaign.

743

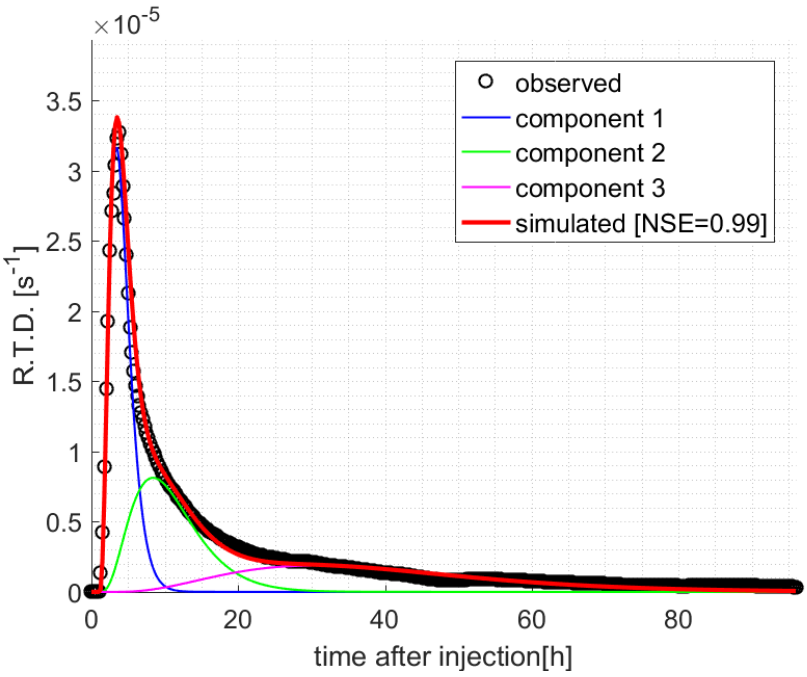

744

745 Fig. 4:

746 Experimental RTD and simulated RTD curves. The simulated curve is composed of 3 sub-
747 functions, called from component 1 to component 3, corresponding respectively to 40%, 32%
748 and 28% of the total solute transport.

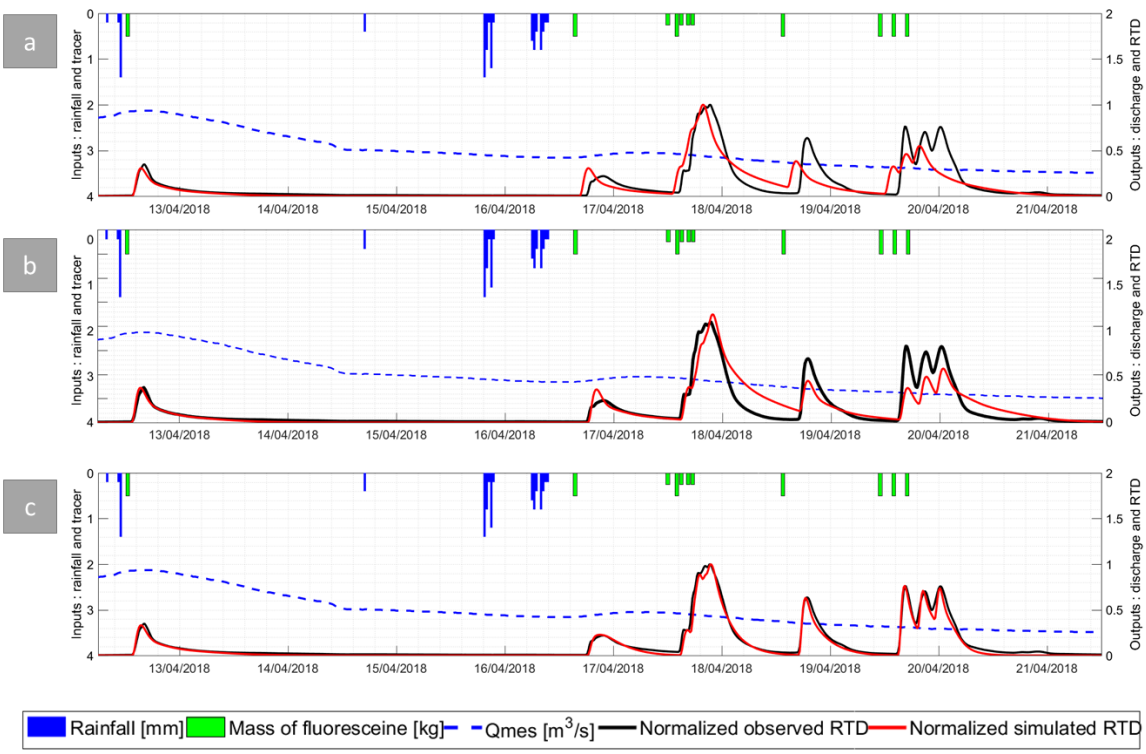

749

750 Fig. 5:

751 Experimental RTD and simulated RTD curves: a) hypothesis: the system is linear and transit
752 time is independent of discharge rate, b) hypothesis: the system is linear and transit time is
753 dependent on discharge rate and c) hypothesis: the system is non-linear, both transit time
754 and mixing coefficient are dependents from discharge rate.

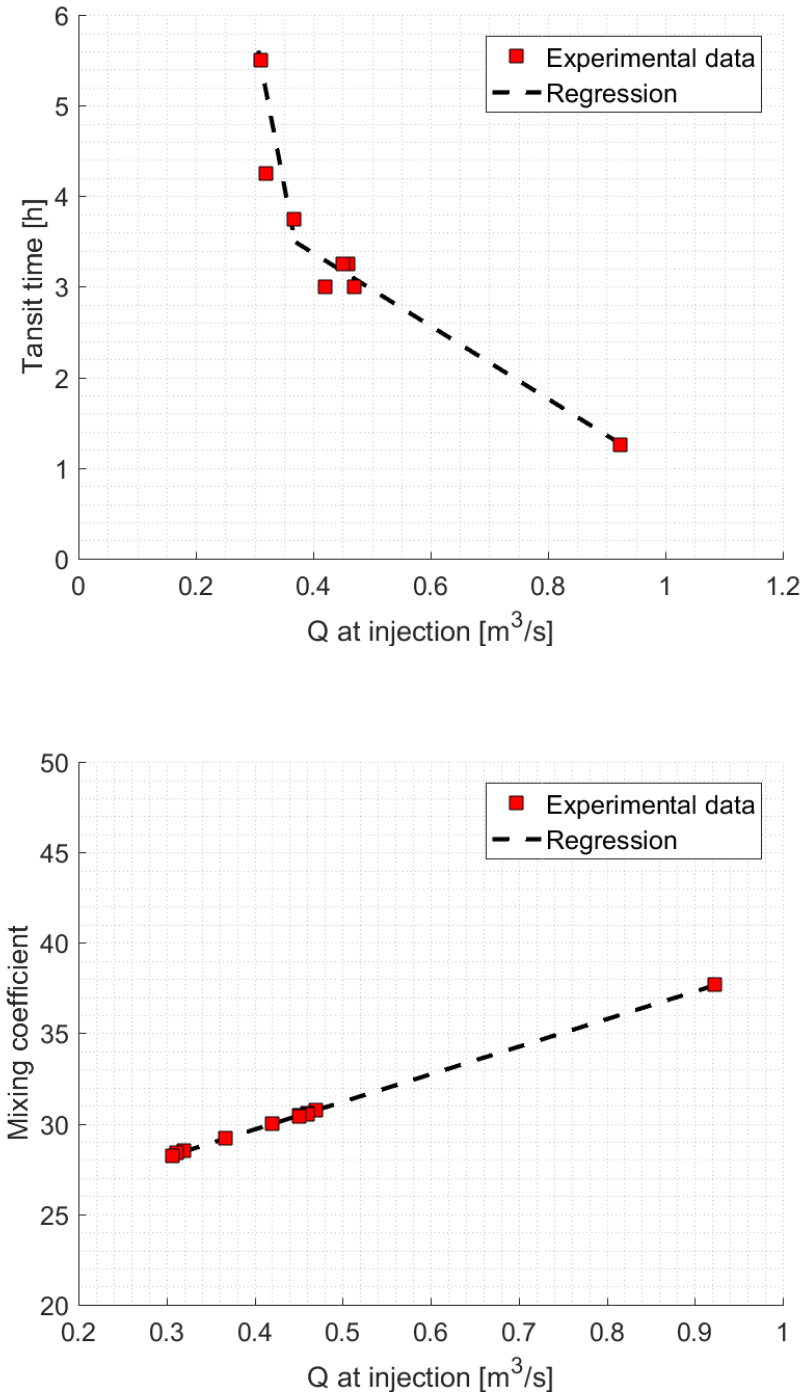

Fig. 6:

Regression between boundary conditions dependent parameters of the transfer function and the outlet discharge rate at the time of injection of the tracer in P2 loss. As all tracer tests were performed in close hydrological conditions and as there was no important influence of rainfall, the outlet discharge is assumed to be representative of the boundary conditions.

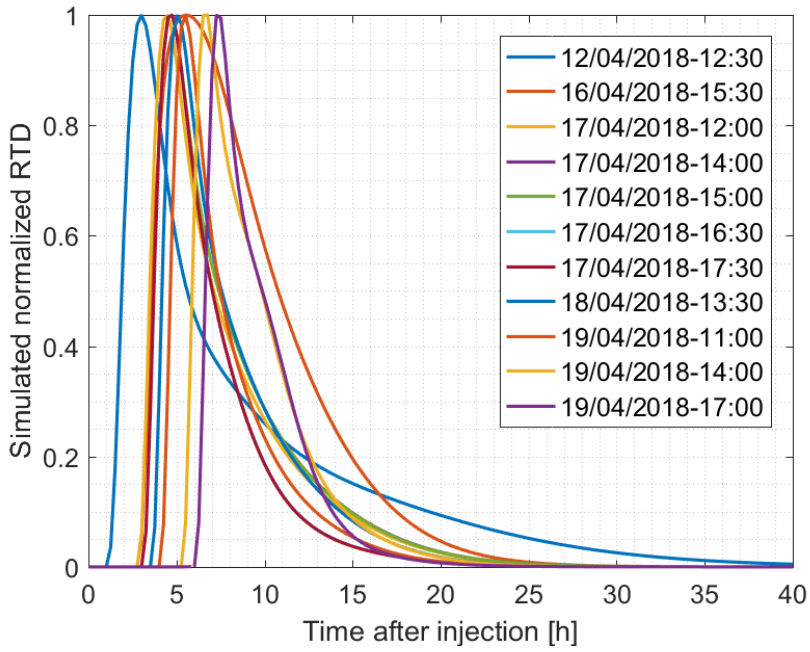

760

761 Fig. 7:

762 Simulated RTD for each of the 11 tracer tests and the corresponding date of injection.

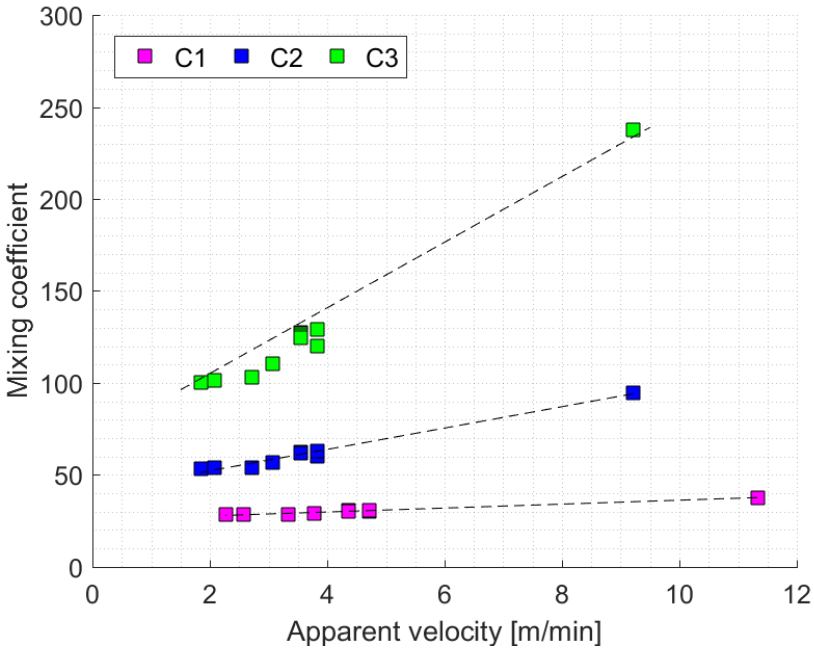

763

764 Fig. 8:

765 Regression between mixing coefficient, noted A in the transfer function, and the apparent

766 velocity.

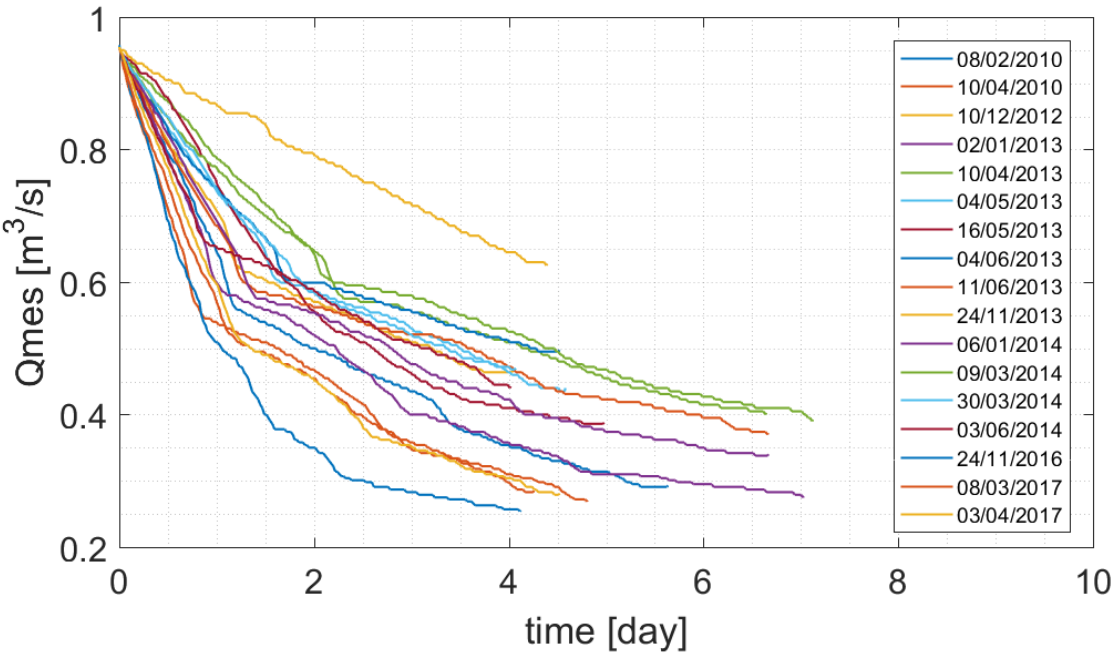

Fig. 9:

Recessions like the one studied through tracer tests observed over the Baget karstic watershed between January 2009 and April 2018: the recession last more than 4 days, the initial discharge is about 0.900 m^3/s and final discharge is above 0.300 m^3/s. So, the scenario of pollution is tested in conditions close to the one investigated field campaign.

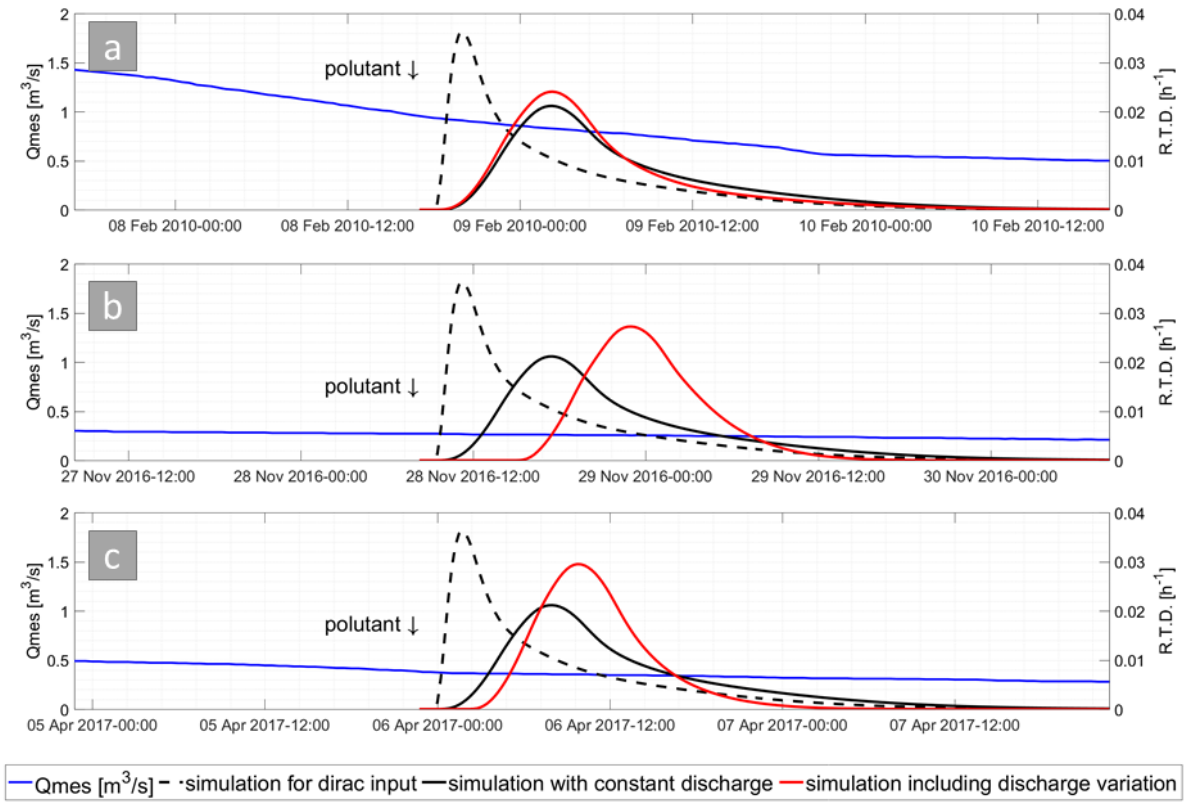

Fig. 10:

Residence time distribution estimated from the model for a constant injection lasting 6 hours. The black arrow corresponds to the beginning of the simulated injection, the black dashed lines represent the impulse response derived from the calibration tracer test, black lines represent the response to a six hours long continuous injection using transfer function regardless discharge variations and red lines represent response including dependence from the outlet discharge.

Test	Date	Mass injected (g)	Q (m^3/s)	Sampling rate (min)
01	12/04/2018 12h30	500	0.923	15
02	16/04/2018 16h30	500	0.421	15
03	17/04/2018 12h00	250	0.470	15
04	17/04/2018 14h00	500	0.460	15
05	17/04/2018 15h00	250	0.460	15
06	17/04/2018 16h30	250	0.450	15
07	17/04/2018 17h30	250	0.450	15
08	18/04/2018 13h30	500	0.367	15
09	19/04/2018 11h00	500	0.320	15
10	19/04/2018 14h00	500	0.311	15
11	19/04/2018 17h00	500	0.306	15

782

783 Table 1:

784 Mass injected and hydrological conditions for each tracer injections.

$\alpha 1$ (%)	A1	$\tau 1$ (H)	$\alpha 2$ (%)	A2	$\tau 2$ (H)	$\alpha 3$ (%)	A3	$\tau 3$ (H)
36	2.51	1.25	30	6.31	1.54	34	15.85	1.83
20	2.00	3.00	38	4.00	3.69	42	8.00	4.38
40	2.05	3.00	32	4.20	3.69	27	8.60	4.38
40	2.04	3.25	32	4.16	4.00	27	8.49	4.75
40	2.04	3.25	32	4.15	4.00	27	8.45	4.75
49	2.03	3.25	39	4.12	4.00	12	8.37	4.75
49	2.03	3.25	39	4.10	4.00	12	8.31	4.75
43	1.95	3.75	31	3.79	4.61	26	7.38	5.48
52	1.90	4.25	30	3.61	5.23	18	6.86	6.21
46	1.89	5.50	40	3.58	6.82	14	6.77	8.15
55	1.88	6.25	40	3.55	7.69	5	6.68	9.13

785

786 Table 2:

787 Parameters of the transfer function for all tracer tests. The simulated RTD is obtained by
788 summation of the contribution of 3 sub-functions where α [%] is the contribution of the total
789 mass transport, A is the mixing coefficient – dependent from outlet discharge – and τ [h] is
790 transit time between input and outlet of the tracing system.